Estimation and characterisation of the wave-induced turbulent kinetic energy and turbulent dissipation from ADCP data

Clément Calvino, Lucille Furgerot, Emmanuel Poizot, Pascal Bailly du Bois, Anne-Claire Bennis

Abstract—**Turbulence in the water flow causes small-scale variations in the mechanical stress acting on submerged tidal turbines. As such it increases their fatigue loading and impacts greatly their lifetime. It is therefore essential for engineers to have an accurate knowledge and characterisation of turbulence at a given site as they design the structures to be deployed. The strength of the tidal currents is the main parameter influencing the intensity of turbulence through their friction with the sea bed. However, most potential tidal energy sites are located in a coastal environment with shallow enough water depths so that the direct impact of waves on turbulence can not be overlooked. Steepness-induced wave breaking is indeed observed to increase the turbulent mixing for such applications. In this context, we propose to estimate the contribution of surface processes to the total turbulence in Alderney Race, France, the most energetic tidal site in western Europe. The turbulent kinetic energy (TKE) specifically induced by waves and wind is characterised using measurements from a 5-beams ADCP deployed between 27/02/2018 and 06/07/2018. Analytical profiles are fitted to the data, the only fitting parameter of the model is an evaluation of the turbulence penetration depth, it determines how deep surface processes impact the water column. Its dependence towards mean wave and current parameters is studied. The results do not allow to conclude on the nature of turbulence observed in the mid water column.**

Index Terms—**Alderney Race, data analysis, turbulent kinetic energy, wave turbulence, Acoustic Doppler Current Profiler**

This work was supported by the French Agence Nationale de la Recherche (ANR), under grants ANR-21-ASM1-0003 (project MORHOC'H 2), and ANR-10-IEED-0006-07 (project HYD2M).

Clément Calvino is at the Morphodynamique Continentale et Côtière (M2C) Laboratory, UMR 6143 M2C, University of Caen-Normandy, 24 rue des Tilleuls, 14000 Caen, Normandie, France (e-mail: clement.calvino@unicaen.fr).

Lucille Furgerot is at the Morphodynamique Continentale et Côtière (M2C) Laboratory, UMR 6143 M2C, University of Caen-Normandy, 24 rue des Tilleuls, 14000 Caen, Normandie, France (e-mail: lucille.furgerot@unicaen.fr).

Emmanuel Poizot is at the Laboratoire Universitaire des Sciences Appliquées de Cherbourg (LUSAC), EA 4253 LUSAC CNAM-INTECHMER, University of Caen-Normandy, 60 rue Max-Pol Fouchet, 50130 Cherbourg-en-Cotentin, Normandie, France (e-mail: emmanuel.poizot@lecnam.net).

Pascal Bailly du Bois is at the Laboratoire Universitaire des Sciences Appliquées de Cherbourg (LUSAC), EA 4253 LUSAC CNAM-INTECHMER, University of Caen-Normandy, 60 rue Max-Pol Fouchet, 50130 Cherbourg-en-Cotentin, Normandie, France (e-mail: pascal.baillydubois@lecnam.net).

Anne-Claire Bennis is at the Morphodynamique Continentale et Côtière (M2C) Laboratory, UMR 6143 M2C, University of Caen-Normandy, 24 rue des Tilleuls, 14000 Caen, Normandie, France (e-mail: anne-claire.bennis@unicaen.fr).

Digital Object Identifier:
https://doi.org/10.36688/ewtec-2023-299

I. Introduction

In the effort of tackling climate change and reducing worldwide carbon emissions, marine renewable energy has regained interests in state policies. For instance the new project FloWatt (https://www.flowatt.fr/) has been proposed in France, planning to install a pilot tidal turbine farm in Alderney Race, the most energetic coastal site in the English Channel. Accurate knowledge of the physical processes inducing mixing in the water column is a key element for dimensioning such structures, and is still an ongoing research topic. Bottom friction between the sea bed and tidal currents (e.g. [1]) and the action of wind stress at the surface (e.g. [2], [3]) have both been extensively studied, they generate wall layers respectively near the sea-bed and near the free surface. In the frame of marine renewable energy the effect of the sea state on the turbulent mixing has regained attention.

All studies agree that wave breaking, either depth-induced or steepness-induced, is the main reason for the increase in TKE and dissipation observed near the free surface (e.g. [4]–[10]). The turbulent dissipation in such a wave breaking affected region is then equal to the energy lost by waves due to breaking. Authors of [7], [11] highlight that the two processes are however very distinct, they lead to different profiles and most of all different scaling for the dissipation. Due to the location of the ADCP data used here we will only retain the steepness-induced case in this manuscript.

Authors of [9] in their Figure 1 or of [8] in their Figure 15 remind clearly how wave breaking impact the balance of turbulent energy. In a first wave breaking layer the transfer of momentum from the waves to the ocean occurs, then TKE is transported downwards in a wave-affected surface layer until a certain depth where the log law is found and shear production balances dissipation. The wind stress layer eventually transitions either to a mixed layer, or more commonly in coastal applications directly to a bottom boundary layer. In each layer a different scaling is assumed for the dissipation, their width also depends on the significant wave height H_s and flow conditions.

The dissipation ϵ is first assumed constant in the wave breaking layer. Authors of [12] find a transition from the wave breaking to the wave-affected layer at $z = 0.6H_s$, where z is the depth pointing downwards with reference $z = 0$ at the mean sea level. With the same scaling [13] finds a close value of $z = 0.5H_s$

and [8] a smaller value of $z = 0.4H_s$. In the wave-affected layer the dissipation follows the scaling given by Eq. (1), with F the wind energy input also identified as the wave dissipation due to breaking under the assumption of stationary wave field:

$$\frac{\epsilon H_s}{F} = c\left(\frac{z}{H_s}\right)^{-b}. \tag{1}$$

The constants c and b are evaluated to 0.3 and 2 respectively in [12]. The wind input is parameterised with the surface friction velocity $u_{\tau,s}$ such as $F = \alpha u_{\tau,s}$, with α a scaling constant usually taken to between 60 and 250 depending on the study (e.g. [4], [5], [7]–[9], [12], [14]). The wind-affected layer lower limit is found by equating Eq. (1) with the classic log law, Eq. (3):

$$z = bH_s\kappa\alpha, \tag{2}$$

where κ is the von Kármán constant. At this depth the turbulence generated by breaking waves and transported downwards matches the local shear production [8], [12]. The log law then predicts a dissipation scaling as follows:

$$\epsilon = \frac{u_{\tau,s}^3}{\kappa z}. \tag{3}$$

The third transition between the surface wind log layer and the bottom friction log layer depends on the ratio between surface and bottom friction velocities ($u_{\tau,b}$). By equating both log laws reminded with Eqs. (3,5) it is found at the following depth:

$$z = \frac{h}{u_{\tau,s}^3/u_{\tau,b}^3 + 1}. \tag{4}$$

In the bottom layer the dissipation scales as Eq. (5), where z' is the height above sea bed obtained by $z' = h - z$, with h the mean total sea level:

$$\epsilon = \frac{u_{\tau,b}^3}{\kappa z'}. \tag{5}$$

The scaling offered for the wind and bottom layers with Eqs. (3,5) neglects the impact of roughness, which is valid as long as we are located far enough from the boundary. It also relies on a balance between shear production and dissipation, neglecting any other process. For instance [15] and later [9] offer an analytical model for the TKE profiles based on a balance between shear production, dissipation, but also vertical transport, with a clear improvement compared to a sole log law model.

Authors of [10] argue that a constant estimate of transition layer is hardly viable, especially in realistic sea states where the size of breakers might vary, therefore mixing both transport of TKE and direct injection near the surface. Most of the studies cited previously indeed focus only on weak wind sea conditions, with measurements located in bays or lakes. These areas are sheltered from well-developed swell in either shallow or very shallow waters between $3\,\mathrm{m}$ and $15\,\mathrm{m}$ depth rarely featuring wave heights more than $1\,\mathrm{m}$ and mean periods longer than $4\,\mathrm{s}$ (e.g. [5], [8], [10], [12]). Authors of [9] demonstrate that in case of a mixed sea state the wind sea significant wave height offer a better scaling with Eq. (1), the full spectrum significant wave height should not be used. The existence of all three layers is not guaranteed and depends on the total depth and forcing conditions. For instance [8] find a direct transition from the wave-affected surface layer to the bottom boundary layer (mean depth of $2.5\,\mathrm{m}$) while [10] observe clearly the wind log layer in between (mean depth of $14\,\mathrm{m}$).

Due to the location of measurement towers in previously cited studies only weak energetic environment are featured, with mean depth-averaged velocities less than $0.5\,\mathrm{ms}^{-1}$. Although rarely mentioned it those studies, such conditions allow to separate clearly bottom processes from surface processes. Alderney Race, the study site for this present research is on the other hand strongly energetic, measured barotropic velocities can reach $3\,\mathrm{ms}^{-1}$ and [16] find peak spring currents around $5\,\mathrm{ms}^{-1}$ through numerical simulations. Authors of [17] offer a breakdown of a vast number of measurements carried out in 2017 and 2018. The area is in particular exposed to Atlantic swell and storms, the sea state is therefore in general dominated by swell with mean periods longer than $10\,\mathrm{s}$ and average wave height of $1.3\,\mathrm{m}$ reaching $8\,\mathrm{m}$ during the strongest storms. Alderney Race is also subject to strong winds with intensity higher than $6.5\,\mathrm{ms}^{-1}$ half of the time. As a result the turbulence generated in the surface and bottom boundary layers are likely to merge and mix in the mid water column, as shown in a previous work on the same site with the same ADCP data [18]. Or said differently the current conditions and current generated turbulence are likely to impact the injection, production, dissipation and transport of turbulent energy even near the surface. It is also well known that wave steepness increases with opposing currents, causing more wave breaking and therefore turbulent injection (e.g. [19]).

The underlying hypothesis and interrogation of the research presented here is a possible linear separation between surface and bottom boundary processes. Indeed the same method used in [18] is reproduced, we estimate the wave and wind contribution $k_{t,\text{surface}}$ to the total TKE $k_{t,\text{total}}$ as per the rationale below, where $k_{t,\text{bottom}}$ is predicted based only on the mean barotropic velocity and attributed solely to the interaction between tidal currents and the sea bed:

$$k_{t,\text{surface}} = k_{t,\text{total}} - k_{t,\text{bottom}}. \tag{6}$$

The surface component is studied, we verify if the scaling given by [12] holds in such an energetic environment, we provide analytical formulas for the TKE profiles and study their dependencies towards wave and tidal mean parameters.

Section II summarises briefly how the data is acquired, processed and how the bottom tidal component of the TKE is extracted. Further theoretical background is reminded in Section III, justifying the method and choices made to evaluate all the variables of interest and to address the questions mentioned previously. The results are presented in Section IV, and discussed in Section V.

Instrument	ADCP Sentinel V50 5 beams
Campaign	Leg56
Deployment period	27/02/2018–06/07/2018
Latitude (°N)	49.68100
Longitude (°E)	−2.02965
Water depth (MSL) (m)	37.7
Beam frequency (kHz)	500
Sampling frequency (Hz)	2
Burst duration (min)	20
Burst frequency (min)	60
Vertical resolution (m)	1
Range (m)	2.7–27.7
Beam inclination (°)	25

TABLE I
ADCP SET-UP PARAMETERS.

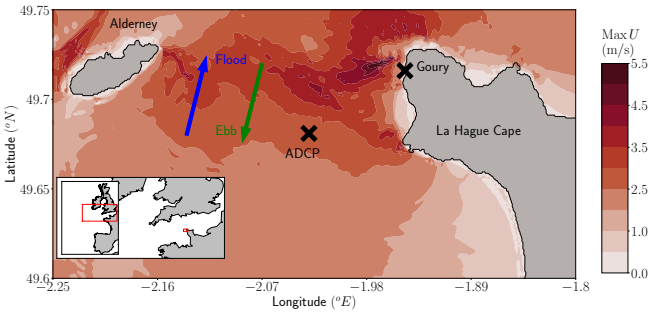

Fig. 1. Map of Alderney Race showing the peak spring currents in the area using data from [16], the calculations are performed during two moon cycles between 01/03/2015 and 29/04/2015; the position of the ADCP used in this research is marked by a red cross; red and orange arrows indicate the respective direction of flood and ebb flows.

II. DATA ACQUISITION AND PROCESSING

Contrary to most references mentioned in introduction where Acoustic Doppler Velocimeter (ADV) measurements are used, we rely here on data gathered by a five-beam ADCP bottom-deployed in Alderney Race. The advantage of using such data is the obtention of a better profile over the water column, with more vertical points. However the drawback is a lower frequency resolution, which is especially damageable when estimating the TKE and dissipation. Additional information on the measurement campaign is given in [17] where the set of data is referred as ADCP S1 Leg56, more details on how the different variables are acquired is also given in [18].

A. ADCP data

Table I summarises the ADCP set-up parameters and campaign information. Figure 1 shows a map of Alderney Race with the position of the ADCP and remind briefly the hydrodynamic characteristics of the area. Beam velocities and sea level are available and recorded with a 2 Hz frequency during 20 min burst windows, between 27/02/2018–06/07/2018. The maximum range of bin heights is between 2.7 m and 27.7 m above the sea bed with a 1 m bin resolution. For the period of measurement the mean sea level is 37.7 m, and the maximum tidal range is 8.2 m, as such the ADCP is able to measure correctly starting at 12 m depth for flood cases at best, and 7 m depth for ebb cases. The data is cleaned by removing low quality measurement points, the method presented in [20] is applied to remove spikes, gaps are then filled with third degree polynomial interpolation over 12 points.

To obtain the mean current parameters the high-resolution data is projected in East-North-Up directions and flat-averaged over each 20 min burst window. This includes the mean sea level and mean velocities. The resolution of the mean sea level is 0.33 m, and the accuracy for the mean velocity is estimated at $0.13\,\mathrm{ms}^{-1}$ [18], which agrees with [21]. The depth-averaged velocities are obtained by averaging over the measured range available, on average 68% of the water column.

The TKE is obtained following [22], the turbulent components of the beam velocities are obtained by removing the flat-average over each 20 min long record window. The data obtained then correspond to a mean statistics, the error still carried by the data is estimated at $0.01\,\mathrm{m}^2\mathrm{s}^{-2}$ [18]. It is worth noting that Doppler noise filtering is not conducted here as the method exposed in [23] and applied in [24], [25] requires to identify the inertial subrange and then flattening of the velocity spectra caused by the noise, which is deemed unreliable with the data at hand due to the poor spectral resolution.

The mean wave parameters are derived from the wave spectra, obtained from the ADCP data using the wave orbital technique. Spectrum partitioning is carried out to evaluate wind sea and swell mean parameters using the watershed algorithm described in [26] as implemented in WAVEWATCH III® [27]. In [17] and [18] the mean wave parameters are estimated with the Teledyne Velocity software [28], however here we recompute those parameters manually from the wave spectra and notably find a bias of −0.16 m on the significant wave heights, specially stronger for extreme events with differences reaching 1 m.

B. Processing and extracting the wave component

Authors of [18] give the full description of the method used to model the tidal-induced TKE, only the main elements are reported here. Flood and ebb cases are treated separately due to different behaviors observed in each case [17], [29], probably caused by a difference in the features encountered by the current flow before reaching the ADCP [30]. For the tidal prediction only cases with $H_s < 0.5\,\mathrm{m}$ are kept so that the effect of sea state can be neglected. For those cases the wind is also weak and always less than $10\,\mathrm{ms}^{-1}$, so the wind log layer is neglected as well. Using this subset of the data the following model is fitted:

$$k_{t,bottom}(z') = A(z')U^p + k_{t,0}(z'), \tag{7}$$

where U is the barotropic velocity, $A(z')$ is the shape profile, $k_{t,0}(z')$ the residual profile and p the velocity scaling coefficient. Those coefficients are evaluated through regressions with the subset of data excluding surface effects, and once known they are used to infer the tidal component $k_{t,bottom}$ of the TKE profiles for all sea state conditions. The surface component of the TKE profiles can then be estimated. The method relies on two major hypothesis, surface effects do not reach deep

enough to modify drastically the bottom tidal profiles, and the mean barotropic velocity is not drastically impacted by surface effects. Those two elements are indeed verified as shown in [18].

III. Theoretical background and method

The turbulent dissipation can be estimated from ADCP measurements, for instance following [24], [31]. Such a method identifies the inertial region characterised by a $-5/3$ log slope on the velocity spectra in order to deduce the dissipation. It requires a smooth spectrum to do so, which is only obtained through an average over several record windows of similar tidal velocity as it is the main physical process generating turbulence. It is therefore not possible to use this method in our study focused on surface processes since the average over velocity bins is also averaging different sea conditions that we specifically want to differentiate. Instead we use Eqs. (8, 9) to estimate the dissipation from the TKE, with c_μ^0 and L empirical parameters, taking the values $c_\mu^0 = 0.09$ and $L = \kappa$ in case of a rigid boundary, and $z_{0,s}$ a surface roughness height:

$$\epsilon = {c_\mu^0}^{3/4} k_t^{3/2} / l_m, \tag{8}$$

$$l_m = L(z + z_{0,s}). \tag{9}$$

Like in many other ocean studies (e.g. [32]–[35]), turbulence in Alderney Race is strongly anisotropic [18]. As such Eq. (8) possibly overestimates the dissipation as it is derived for isotropic turbulence in the inertial subrange. For instance a better agreement is found in [18] when using an estimate of isotropic turbulence from the vertical TKE only. A different approach is conducted in several studies (e.g. [9], [10]) where the constants c_μ^0 and L are allowed to vary and fitted to the data, for instance through an analytical expression of the TKE profile. Assuming a balance between shear production, dissipation and transport such an expression is given in [9], [13], [15], reminded with Eq. (10):

$$k_t^{3/2} = \frac{u_{\tau,s}^3}{{c_\mu^0}^{3/4}} + \frac{F}{2}\left(\frac{3\sigma_{k_t}}{2c_\mu}\right)^{1/2}\left(\frac{z}{z_{0,s}}\right)^{-m}, \tag{10}$$

with σ_{k_t} the Schmidt number for TKE and c_μ another tuning constant and m related to the mixing length parameter L as follows:

$$m = \frac{{c_\mu^0}^{3/4}}{L}\left(\frac{3\sigma_{k_t}}{2c_\mu}\right)^{1/2}. \tag{11}$$

To simplify the analysis a consensus is to assume $\sigma_{k_t} = 1$ and $c_\mu = c_\mu^0$, although those choices could easily be argued [10]. The wind friction velocity $u_{\tau,s}$ is still needed, we use the formulation of [2], corrected in [36], with W_{10} the $10\,\mathrm{m}$ height wind magnitude (from the MétéoFrance station installed at the Goury semaphore), $W_r = 31.5\,\mathrm{ms}^{-1}$ a model constant and ρ_a the air density, ρ the water density:

$$u_{\tau,s}^2 = \frac{\rho_a}{\rho}\left(0.55 + 2.97\frac{w_{10}}{w_r} - 1.49{\frac{w_{10}}{w_r}}^2\right)10^{-3} w_{10}^2, \tag{12}$$

The remaining free parameters for the model are then L, varying between 0.2 and 0.4 in the literature, c_μ^0, varying between 0.09 and 0.20 and finally $z_{0,s}$ of the order of H_s, in accordance to Eq. (2).

The scaling law of [12] reminded with Eq. (1) still requires the wave energy input from whitecapping F. It can either be estimated from the surface friction velocity directly (e.g. [4], [5], [9], [12]) or from the wave spectrum often assuming a stationary state where the wind input equals the wave breaking dissipation in the water column (e.g. [8], [10], [37]). Since we have access to wave spectral data we opt for the second solution, however we decide to directly estimate the breaking dissipation from the wave spectra so we don't need to rely on any assumption on the wave field. The nonlinear saturation-based model of [38] is used, it reads:

$$F = \int_{\sigma=0}^{\infty}\int_{\theta=0}^{2\pi} c_F \left(\frac{B(k)}{B_r}\right)^{p_F/2} g^{1/2}k^{1/2}E(\sigma,\theta)\,\mathrm{d}\theta\mathrm{d}\sigma, \tag{13}$$

with E the variance density spectrum, $c_F = 5\cdot 10^{-5}$ and $B_r = 1.75\cdot 10^{-3}$ default tuning constants, θ the spectral wave direction, σ the intrinsic wave frequency, k the wavenumber and $B(k)$ is the spectral saturation spectrum computed as follows:

$$B(k) = \int_{\theta=0}^{2\pi} \frac{\mathrm{d}\sigma}{\mathrm{d}k} k^3 E(\sigma,\theta)\,\mathrm{d}\theta, \tag{14}$$

the exponent p_F takes the form:

$$p_F = \frac{p_0}{2}\left(1 + \tanh\left[10\left(\left(\frac{B(k)}{B_r}\right)^{1/2} - 1\right)\right]\right), \tag{15}$$

with p_0 estimated as follows, using $w = 26$:

$$p_0 = 3 + \tanh\left[w\left(\frac{u_{\tau,s}k}{\sigma} - 0.1\right)\right]. \tag{16}$$

IV. Results

The model proposed with Eq. 7 is applied to the ADCP data as explained in Section II, separating flood and ebb cases. Table II gives the fitted parameters for the model. The surface-induced TKE is then computed using Eq. (6) for each profile obtained through one $20\,\mathrm{min}$ long record window. Figure 2 shows the surface-induced TKE profiles for both flood and ebb cases. For clarity only samples with total significant wave height $H_s > 1.5\,\mathrm{m}$ are kept.

The roughness height $z_{0,s}$ only is estimated through a brute optimisation method based on the analytical profiles given by Eqs. (10, 11). The surface friction velocity $u_{\tau,s}$ and wind energy input F are computed directly from the data, as exposed in Section III, while several fixed values of c_μ^0 and L are tested as detailed in Table III. As observed in Figure 2, the few last meters below the surface are never exploitable by the ADCP, which is even more true for the flood cases due to higher mean sea levels. We then restrain the analysis to cases with at least $H_s > 1.5\,\mathrm{m}$ in order to have a noticeable impact of surface effects, hopefully reaching deep enough with a wave-induced magnitude

	Flood			Ebb		
z'	$A(z')$	$k_{t,0}(z')$	p	$A(z')$	$k_{t,0}(z')$	p
2.7	0.0087	0.0040	2.01	0.0157	0.0030	1.92
3.7	0.0086	0.0041	2.01	0.0161	0.0031	1.92
4.7	0.0084	0.0045	2.01	0.0155	0.0038	1.92
5.7	0.0083	0.0045	2.01	0.0145	0.0043	1.92
6.7	0.0081	0.0047	2.01	0.0131	0.0050	1.92
7.7	0.0077	0.0051	2.01	0.0119	0.0056	1.92
8.7	0.0075	0.0053	2.01	0.0110	0.0060	1.92
9.7	0.0072	0.0054	2.01	0.0104	0.0061	1.92
10.7	0.0068	0.0057	2.01	0.0099	0.0063	1.92
11.7	0.0066	0.0058	2.01	0.0094	0.0064	1.92
12.7	0.0063	0.0060	2.01	0.0089	0.0067	1.92
13.7	0.0060	0.0061	2.01	0.0084	0.0068	1.92
14.7	0.0056	0.0063	2.01	0.0081	0.0070	1.92
15.7	0.0052	0.0065	2.01	0.0076	0.0074	1.92
16.7	0.0048	0.0066	2.01	0.0073	0.0074	1.92
17.7	0.0045	0.0068	2.01	0.0069	0.0076	1.92
18.7	0.0041	0.0071	2.01	0.0065	0.0079	1.92
19.7	0.0038	0.0074	2.01	0.0062	0.0080	1.92
20.7	0.0034	0.0079	2.01	0.0059	0.0083	1.92
21.7	0.0031	0.0083	2.01	0.0056	0.0087	1.92
22.7	0.0027	0.0087	2.01	0.0052	0.0090	1.92
23.7	0.0024	0.0090	2.01	0.0048	0.0097	1.92
24.7	0.0021	0.0095	2.01	0.0044	0.0104	1.92
25.7	0.0018	0.0098	2.01	0.0041	0.0109	1.92
26.7	0.0016	0.0101	2.01	0.0037	0.0114	1.92
27.7	0.0014	0.0103	2.01	0.0033	0.0123	1.92

TABLE II
TKE MODEL PARAMETERS GIVEN BY EQ. (7).

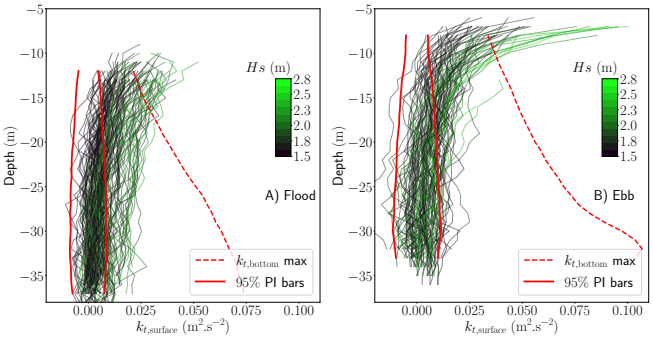

Fig. 2. Surface-induced TKE profiles for flood (A) and ebb (B) cases showing only samples with $H_s > 1.5\,\text{m}$ for clarity, profiles are coloured by the significant wave height ; the red bars correspond to the 95% prediction interval for the tidal generated TKE model.

stronger than error levels. For the same reason we also select profiles where the maximum number data points is available, around 25, which allows for meaningful modelling of the profiles. Table III shows the mean statistics for the different choices of tuning constants c_μ^0 and L, separating flood and ebb cases. The Root-Mean-Square Errors (RMSE) are always low, half the uncertainty levels attributed to the measurement and processing errors. However the correlation coefficients are quite low, 0.859 at best for ebb cases and below 0.777 for flood cases. It indicates that on average the profiles are still badly captured by the model. Small differences, less than 0.01, are observed between the statistics depending on the constant parameters. There is a mild indication that $L = 0.3$ gives the best agreement overall. For ebb cases the best agreement is then for $c_\mu^0 = 0.21$ and $c_\mu^0 = 0.09$ for flood cases, although differences are almost negligible.

Two profiles of surface-induced TKE for flood

	Flood, 76 profiles		Ebb, 67 profiles	
	RMSE (m^2/s^2)	R	RMSE (m^2/s^2)	R
$c_\mu^0 = 0.09, L = 0.2$	0.0051	0.772	0.0053	0.858
$c_\mu^0 = 0.09, L = 0.3$	0.0053	0.777	0.0056	0.856
$c_\mu^0 = 0.09, L = 0.4$	0.0058	0.776	0.0063	0.850
$c_\mu^0 = 0.13, L = 0.2$	0.0053	0.769	0.0054	0.856
$c_\mu^0 = 0.13, L = 0.3$	0.0055	0.777	0.0055	0.858
$c_\mu^0 = 0.13, L = 0.4$	0.0058	0.776	0.0061	0.852
$c_\mu^0 = 0.17, L = 0.2$	0.0055	0.766	0.0055	0.854
$c_\mu^0 = 0.17, L = 0.3$	0.0055	0.776	0.0054	0.858
$c_\mu^0 = 0.17, L = 0.4$	0.0059	0.776	0.0060	0.854
$c_\mu^0 = 0.21, L = 0.2$	0.0057	0.764	0.0056	0.852
$c_\mu^0 = 0.21, L = 0.3$	0.0056	0.775	0.0053	0.859
$c_\mu^0 = 0.21, L = 0.4$	0.0059	0.776	0.0059	0.855

TABLE III
RMSE AND CORRELATION COEFFICIENT R FOR THE OPTIMISED ANALYTICAL TKE PROFILE DEFINED WITH EQ. 10 AGAINST THE SURFACE-INDUCED TKE DATA, AVERAGED OVER ALL PROFILES WITH AT LEAST 25 DATA POINTS AVAILABLE AND $H_s > 1.5\,\text{m}$.

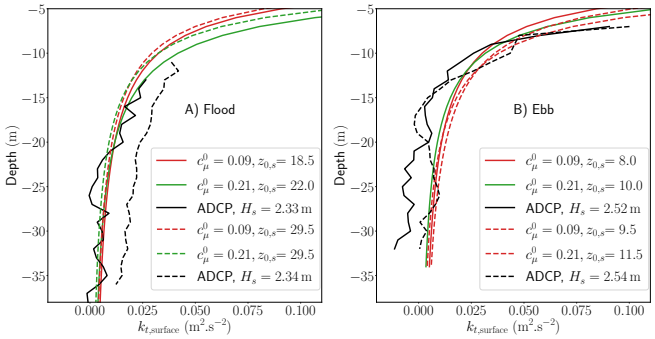

Fig. 3. Two surface-induced TKE profiles for flood (A) and ebb (B) with their optimised model estimation according to Eq. 10, the black lines are the profiles directly estimated from ADCP data, the red lines the model with $c_\mu^0 = 0.09, L = 0.2$ and the green lines with $c_\mu^0 = 0.09, L = 0.2$.

and ebb, coinciding with the highest total significant heights, are presented on Figure 3. The two best configurations with $L = 0.3$, $c_\mu^0 = 0.09$ or $c_\mu^0 = 0.21$, are plotted as well with the optimised value of $z_{0,s}$. The profiles are expanded on purpose above the range of available measurements. For flood cases the sharp increase due to surface processes appears precisely above this range, which explains why in general a worse agreement is found. Suspiciously high values of $z_{0,s}$ are also found for those flood cases, and in general for all flood cases. As a result we decide to focus solely on the ebb cases. The surface roughness heights are still high, around $10\,\text{m}$, however it corresponds well with the behavior observed on the data. The strongest discrepancies appear for the homogeneous part of the profiles, below $10\,\text{m}$ depth, they are mostly explained by the measurement and processing errors of the order of $0.01\,\text{m}^2\text{s}^{-2}$.

The dependence of $z_{0,s}$ towards the wind wave partition significant wave height (plot A), the wind wave partition peak period (plot B) and the mean barotropic current (plot C) is shown with Figure 4. No obvious trend is observed, or if any a negative correlation with the significant wave height, which goes against the expectation and against Eq. (2). Not shown here, using

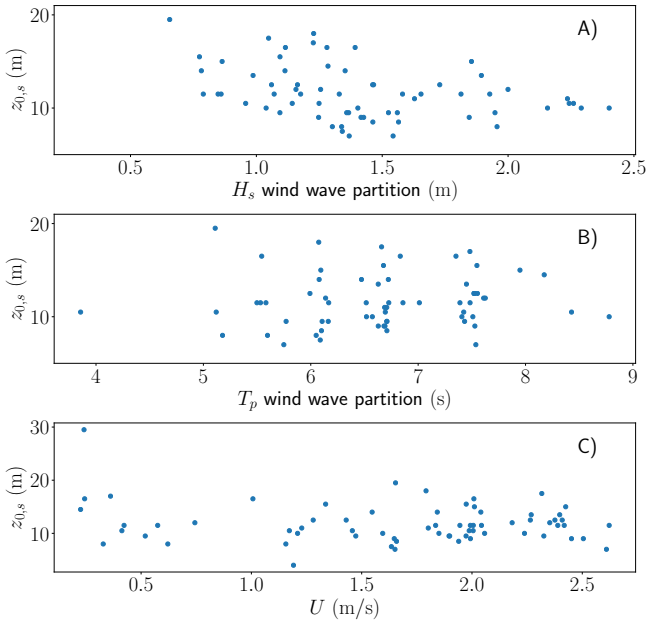

Fig. 4. Scatter plots of $z_{0,s}$ as a function of the wind wave partition significant wave height H_s, peak period T_p, and mean current U.

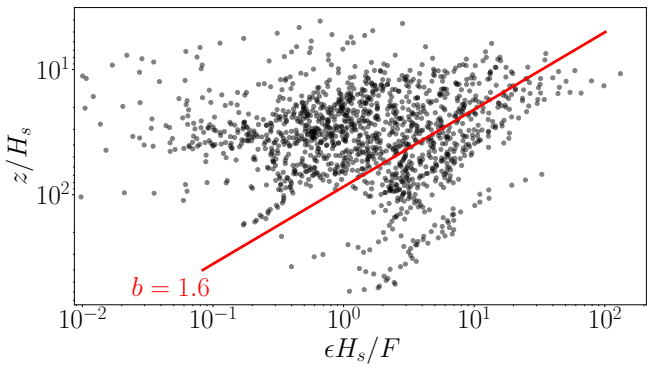

Fig. 5. Collapse of the scaled dissipation on the scaled depth, the red line shows the averaged linear regression according to Eq. (1) with $b = 1.6$.

the total or swell partition mean parameters does not show any trend either.

Finally the scaling proposed with Eq. (1) is tested and illustrated with Figure 5. A large spread on the data is observed, for each individual profile a scaling is still relevant, however the data does not collapse on a single line as expected from the theory. The average log law is found for $b = 1.6$, with values ranging from $b = 0.13$ to $b = 3.12$.

V. Discussion

Neither the analysis of the TKE profiles nor the dissipation give satisfying and clear results. The fitted value of $z_{0,s}$ is too high compared to the expectation found in the literature, at best of the order of H_s [10], and the values do not behave at all like one would expect with respect to mean wave parameters. On a similar note, the scaling of the dissipation with respect to the depth yields a large spread, with a mean power coefficient $b = 1.6$ exactly between the expected value for a wind-shear dominated layer ($b = 1$) and a wave-affected surface layer ($b = 2$). As a result it is not possible to state with certainty whether yes or no the sheared TKE profiles observed in Figure 2 correspond indeed to a wave-affected layer, or a wind log layer. It is likely that both cases can be encountered depending on the environmental conditions, but that would require further analysis and so far no trend has been detected in the data. The lack of clear results is explained by several strong limitations of the method presented in this paper, and relying on ADCP data.

The ADCP was deployed in a deep enough location so that it was difficult to obtain valid and reliable data near the surface. This is a recurring limitation with ADCP campaigns due to surface effects deteriorating the measurements, the 5 first meters below the surface are never exploitable. However due to the decreasing quality of data acquisition with distance to the emitter, even the first 10 meters have to be discarded for flood cases. Moreover the quality of data further from the device is lower, which is especially damaging when studying the TKE. This is due to the beam cells geometrically growing in size, and therefore intrinsically badly capturing the smallest turbulent structures. Putting aside the data quality, the lack of data in the first surface meters, where the transition between the wave-affected surface layer and the wind log layer is expected, prevents a reliable estimation of $z_{0,s}$, as illustrated with Figure 4. Most, if not all, past studies cited in this paper rely on ADV measurements, configured specifically with the intention of characterising the turbulence and often assembled in a turbulence tower. They are often deployed in rather sheltered locations, which allows for measurements close to the sea surface, within those few meters where the transition and shift in dominant turbulent processes happens. As such ADVs are still more suited for such applications. Yet those turbulence towers are hardly usable in harsh environments, like Alderney Race, as the structure could be damaged during strong storms. Bottom-mounted ADCPs on the other hand are unaffected, but the present study indicates that more efforts in calibrating the deployment campaign and in the data processing are needed for near surface turbulent applications.

The friction velocity $u_{\tau,s}$ and wind energy input F are also crucial elements for the analysis conducted in this paper, their quality and trustworthiness can be questioned here. Furthermore we do not posses any other independent way of verifying the values taken by those variables. The wind data in particular is measured around 10 km away from the ADCP on land, on top of a cliff. The wind friction is then probably poorly estimated, and as a result the wave breaking flux as well. This issue is clearly observed in Figure 6. The literature indicates that the wave energy input from breaking should be a linear function of the friction velocity cubed, $F = \alpha u_{\tau,s}^3$, with α a constant varying between 60 and 250 depending on the study (e.g. [4], [5], [7], [9], [12], [14]). However Figure 6 displays a strong spread, with no clear linear trend but lower and upper estimations of α between 3 and 3000. The spread is too large to be explained solely by the exposure of the area to strong winds and swell.

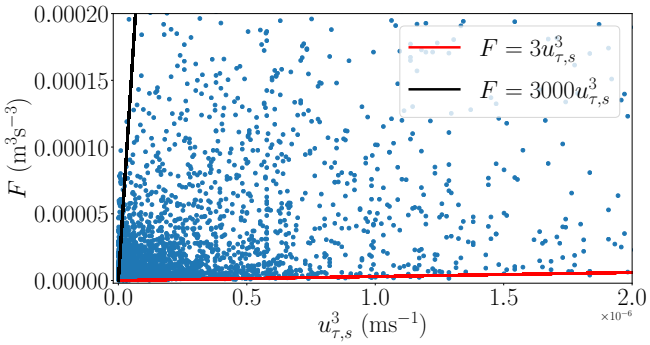

Fig. 6. Scatter plot of the wave breaking energy input F against the surface friction velocity cubed $u^3_{\tau,s}$, the solid lines indicate roughly the upper and lower limits for a linear relationship between the two variables plotted.

Finally all constant parameters and stability functions, such as c^0_μ, L, and σ_{k_t}, are held constant as if one value could fit the whole dataset. As shown in [8] and [10] it is often true for free shear situations, but in general they dependent on the flow characteristics. They are well explained by the dissipation, TKE, stress and shear, which indeed all dependent on the sea state. An accurate choice of those parameters is crucial especially for ADCP derived data, unlike with ADVs the dissipation can not be measured directly and has to be estimated from the TKE through Eqs. (8, 9). This difficulty can also explain the large spread observed in Figure 5. It will notably be the topic of further research to allow those parameters to vary when fitting the profile given by Eq. (10).

APPENDIX
DEFINITION OF STATISTICS

The statistics used in this paper are defined below, they correspond to depth-average values for each individual profile. $X_{\mathrm{o},i}$ corresponds to the observation at bin number i, while $X_{\mathrm{m},i}$ to the model estimate, D is the number of bins where data is available, varying from one profile to the other:

$$\mathrm{RMSE} = \sqrt{\frac{1}{D}\sum_{i=1}^{D}\left(X_{\mathrm{m},i} - X_{\mathrm{o},i}\right)^2}, \tag{17}$$

$$V_{\mathrm{m},i} = X_{\mathrm{m},i} - \frac{1}{D}\sum_{i=1}^{D} X_{\mathrm{m},i}, \tag{18}$$

$$V_{\mathrm{o},i} = X_{\mathrm{o},i} - \frac{1}{D}\sum_{i=1}^{D} X_{\mathrm{o},i}, \tag{19}$$

$$R = \frac{\sum_{i=1}^{D}\left(V_{\mathrm{m},i}\right)\left(V_{\mathrm{o},i}\right)}{\sqrt{\sum_{i=1}^{D}\left(V_{\mathrm{m},i}\right)^2\sum_{i=1}^{D}\left(V_{\mathrm{o},i}\right)^2}}. \tag{20}$$

ACKNOWLEDGEMENT

We wish to acknowledge the crew of the R/V 'Côtes de la Manche' and the support from France Energies Marines (FEM).

REFERENCES

[1] S. B. Pope, *Turbulent flows*. IOP Publishing, 2001.
[2] J. Wu, "Wind-induced drift currents," *Journal of Fluid Mechanics*, vol. 68, no. 1, p. 49–70, 1975.
[3] I. S. F. Jones, *Turbulence Below Wind Waves*. Dordrecht: Springer Netherlands, 1985, pp. 437–442.
[4] P. D. Craig and M. L. Banner, "Modeling wave-enhanced turbulence in the ocean surface layer," *Journal of Physical Oceanography*, vol. 24, no. 12, pp. 2546 – 2559, 1994.
[5] W. M. Drennan, M. A. Donelan, E. A. Terray, and K. B. Katsaros, "Oceanic turbulence dissipation measurements in SWADE," *Journal of Physical Oceanography*, vol. 26, no. 5, pp. 808 – 815, 1996.
[6] E. Terray, W. Drennan, and M. Donelan, "The vertical structure of shear and dissipation in the ocean surface layer," Woods Hole Oceanographic Institution MA Dept of Applied Ocean Physics, Tech. Rep., 1999.
[7] F. Feddersen, J. H. Trowbridge, and A. J. Williams, "Vertical structure of dissipation in the nearshore," *Journal of Physical Oceanography*, vol. 37, no. 7, pp. 1764 – 1777, 2007.
[8] N. L. Jones and S. G. Monismith, "The influence of whitecapping waves on the vertical structure of turbulence in a shallow estuarine embayment," *Journal of Physical Oceanography*, vol. 38, no. 7, pp. 1563 – 1580, 2008.
[9] G. P. Gerbi, J. H. Trowbridge, E. A. Terray, A. J. Plueddemann, and T. Kukulka, "Observations of turbulence in the ocean surface boundary layer: Energetics and transport," *Journal of Physical Oceanography*, vol. 39, no. 5, pp. 1077 – 1096, 2009.
[10] A. W. Fisher, L. P. Sanford, and M. E. Scully, "Wind-wave effects on estuarine turbulence: A comparison of observations and second-moment closure predictions," *Journal of Physical Oceanography*, vol. 48, no. 4, pp. 905 – 923, 2018.
[11] F. Feddersen and J. Trowbridge, "The effect of wave breaking on surf-zone turbulence and alongshore currents: A modeling study," *Journal of Physical Oceanography*, vol. 35, no. 11, pp. 2187–2203, 2005.
[12] E. Terray, M. Donelan, Y. Agrawal, W. Drennan, K. Kahma, A. Williams, P. Hwang, and S. Kitaigorodskii, "Estimates of kinetic energy dissipation under breaking waves," *Journal of Physical Oceanography*, vol. 26, no. 5, pp. 792 – 807, 1996.
[13] H. Burchard, "Simulating the wave-enhanced layer under breaking surface waves with two-equation turbulence models," *Journal of Physical Oceanography*, vol. 31, no. 11, pp. 3133 – 3145, 2001.
[14] A. W. Fisher, L. P. Sanford, M. E. Scully, and S. E. Suttles, "Surface wave effects on the translation of wind stress across the air–sea interface in a fetch-limited, coastal embayment," *Journal of Physical Oceanography*, vol. 47, no. 8, pp. 1921 – 1939, 2017.
[15] P. D. Craig, "Velocity profiles and surface roughness under breaking waves," *Journal of Geophysical Research: Oceans*, vol. 101, no. C1, pp. 1265–1277, 1996.
[16] P. Bailly du Bois, F. Dumas, M. Morillon, L. Furgerot, C. Voiseux, E. Poizot, Y. Méar, and A.-C. Bennis, "The Alderney Race: general hydrodynamic and particular features," *Philosophical Transactions of the Royal Society A: Mathematical, Physical and Engineering Sciences*, vol. 378, no. 2178, p. 20190492, 2020.
[17] L. Furgerot, A. Sentchev, P. Bailly du Bois, G. Lopez, M. Morillon, E. Poizot, Y. Méar, and A.-C. Bennis, "One year of measurements in Alderney Race: preliminary results from database analysis," *Philosophical Transactions of the Royal Society A: Mathematical, Physical and Engineering Sciences*, vol. 378, no. 2178, p. 20190625, 2020.
[18] C. Calvino, L. Furgerot, E. Poizot, P. B. du Bois, and A.-C. Bennis, "Model and method to predict the turbulent kinetic energy induced by tidal currents, application to the wave-induced turbulence," *Renewable Energy*, p. 119024, 2023.
[19] J. Wolf and D. Prandle, "Some observations of wave–current interaction," *Coastal Engineering*, vol. 37, no. 3, pp. 471–485, 1999.
[20] D. G. Goring and V. I. Nikora, "Despiking acoustic doppler velocimeter data," *Journal of Hydraulic Engineering*, vol. 128, no. 1, pp. 117–126, 2002.
[21] T. B. Sanford and R.-C. Lien, "Turbulent properties in a homogeneous tidal bottom boundary layer," *Journal of Geophysical Research: Oceans*, vol. 104, no. C1, pp. 1245–1257, 1999.

[22] R. Dewey and S. Stringer, "Reynolds stresses and turbulent kinetic energy estimates from various ADCP beam configurations: Theory," 2015, unpublished manuscript.
[23] V. Durgesh, J. Thomson, M. C. Richmond, and B. L. Polagye, "Noise correction of turbulent spectra obtained from acoustic doppler velocimeters," *Flow Measurement and Instrumentation*, vol. 37, pp. 29–41, 2014.
[24] J. M. McMillan, A. E. Hay, R. G. Lueck, and F. Wolk, "Rates of dissipation of turbulent kinetic energy in a high Reynolds number tidal channel," *Journal of Atmospheric and Oceanic Technology*, vol. 33, no. 4, pp. 817 – 837, 2016.
[25] M. Thiébaut, J.-F. Filipot, C. Maisondieu, G. Damblans, R. Duarte, E. Droniou, N. Chaplain, and S. Guillou, "A comprehensive assessment of turbulence at a tidal-stream energy site influenced by wind-generated ocean waves," *Energy*, vol. 191, p. 116550, 2020.
[26] L. Vincent and P. Soille, "Watersheds in digital spaces: an efficient algorithm based on immersion simulations," *IEEE Transactions on Pattern Analysis and Machine Intelligence*, vol. 13, no. 6, pp. 583–598, 1991.
[27] The WAVEWATCH III R® Development Group, "User manual and system documentation of WAVEWATCH III R® version 6.07," NOAA, College Park, MD, USA, Tech. Rep. Tech. Note 333, 2019.
[28] E. A. Terray, B. H. Brumley, and B. Strong, "Measuring waves and currents with an upward-looking ADCP," *Proceedings of the IEEE Sixth Working Conference on Current Measurement*, pp. 66–71, 1999.
[29] M. Togneri, M. Lewis, S. Neill, and I. Masters, "Comparison of ADCP observations and 3D model simulations of turbulence at a tidal energy site," *Renewable Energy*, vol. 114, pp. 273–282, 2017, wave and Tidal Resource Characterization.
[30] L. Furgerot, Y. Poprawski, M. Violet, E. Poizot, P. B. du Bois, M. Morillon, and Y. Mear, "High-resolution bathymetry of the Alderney race and its geological and sedimentological description (Raz Blanchard, northwest France)," *Journal of Maps*, vol. 15, no. 2, pp. 708–718, 2019.
[31] M. Guerra and J. Thomson, "Turbulence measurements from five-beam Acoustic Doppler Current Profilers," *Journal of Atmospheric and Oceanic Technology*, vol. 34, no. 6, pp. 1267 – 1284, 2017.
[32] I. Nezu and H. Nakagawa, *Turbulence in open-channel flows*. Taylor & Francis, 1993.
[33] M. T. Stacey, S. G. Monismith, and J. R. Burau, "Measurements of Reynolds stress profiles in unstratified tidal flow," *Journal of Geophysical Research: Oceans*, vol. 104, no. C5, pp. 10 933–10 949, 1999.
[34] J. Thomson, B. Polagye, V. Durgesh, and M. C. Richmond, "Measurements of turbulence at two tidal energy sites in Puget Sound, WA," *IEEE Journal of Oceanic Engineering*, vol. 37, no. 3, pp. 363–374, 2012.
[35] I. A. Milne, R. N. Sharma, R. G. J. Flay, and S. Bickerton, "Characteristics of the turbulence in the flow at a tidal stream power site," *Philosophical Transactions of the Royal Society A: Mathematical, Physical and Engineering Sciences*, vol. 371, no. 1985, p. 20120196, 2013.
[36] M. Zijlema, G. van Vledder, and L. Holthuijsen, "Bottom friction and wind drag for wave models," *Coastal Engineering*, vol. 65, pp. 19–26, 2012.
[37] M. E. Scully, J. H. Trowbridge, and A. W. Fisher, "Observations of the transfer of energy and momentum to the oceanic surface boundary layer beneath breaking waves," *Journal of Physical Oceanography*, vol. 46, no. 6, pp. 1823 – 1837, 2016.
[38] A. J. van der Westhuysen, M. Zijlema, and J. A. Battjes, "Nonlinear saturation-based whitecapping dissipation in SWAN for deep and shallow water," *Coastal Engineering*, vol. 54, no. 2, pp. 151–170, 2007.